Stable multi-layer flows at all Re

Visco-plastic lubrication of shear-thinning and viscoelastic fluids

Miguel Moyers-Gonzalez[1], Ian Frigaard[2], Chérif Nouar[3]

[1] Department of Mathematics and Statistics, University of Canterbury, Private Bag 4800, Christchurch, New Zealand

[2] Department of Mathematics and Department of Mechanical Engineering, University of British Columbia, 1984 Mathematics Road, Vancouver, BC, Canada, V6T 1Z2.

[3] Nancy Université, LEMTA - UMR 7563 CNRS - INPL - UHP, 2, Avenue de la Forêt de Haye, BP 160, 54504 Vandoeuvre-Lès-Nancy, France.

Abstract   Insert your abstract here.

1 Introduction

Multi-layer shear flows arise in at least 3 general areas of industrial application. (i) Co-extrusion processes, in which several fluid streams are combined in a feedblock, from where the combined melt stream flows to a die and the layers take their final dimensions. Co-extrusion processes are extensively used in the production of bilayer and multi-layer sheets and pipes in the plastics industry and the production of conjugate fibres in the fibre industry. Interest in multi-layer extrusion has also grown due to its potential for producing composite products with improved material properties. (ii) Lubricated pipelining, in which an outer layer of low viscosity fluid is used to enhance the flow of an inner fluid. the outer fluid occupies the regions of highest shear adjacent to the walls of the duct. Such processes are used for example where a heavy crude oil is transported along pipelines with the addition of a small amount of water. Similar methods are used in coalwater slurry transport. (iii) Coating flows, in which an additional layer of fluid is applied to the outside of another fluid stream, e.g. in the concentric coating of two or more polymers.

In many of these processes the rate of production (i.e. the flow rate), is limited by flow instabilities and especially by instabilities at the interfaces between adjacent layers. These instabilities can result in high scrap rates, in an economically infeasible process, or in final products

with substandard mechanical, optical or barrier properties. This is the essential motivation for study of these instabilities and of methods to remove or avoid them. This paper presents one such method.

At large Reynolds number, Re, multi-layer flows of viscous fluids are usually unstable. This arises in any case due to the emergence of shear instabilities, i.e. turbulent transition, but linear interfacial instabilities are also found for quite low Re. Dating from the late 1960's, there are a number of studies involving both immiscible and miscible fluids, e.g. [11,12]. An extensive review can be found in the text [13], and the physical mechanisms governing short and long wavelength instabilities have been explained by [14,15]. These studies generally refer to the situation where there is a jump in the viscosity at the interface between two fluids. If the change in viscosity is instead gradual, e.g. due to a diffuse interfacial region, then the stability characteristics appear to mimic those of the system with the viscosity jump, see [16].

A number of authors have considered the stability of multi-layer flows of non-Newtonian fluids. For example, linear stability of multi-layer Couette and Poiseuille flows of power law fluids have been treated extensively in [17–20], both by developing the analogous analytic expressions to the Newtonian fluid problems, and by numerical solution of the linear stability problems. In general terms, these flows suffer from interfacial instabilities of similar nature to those for Newtonian fluids. Although the non-Newtonian rheology can positively in-

fluence the stability, it is not effective in wholly eliminating interfacial instabilities. If the physical mechanism of short wavelength instability described in [14] is accepted, then sufficiently close to the fluid-fluid interface, the non-Newtonian character of these fluids is simply not recognised, (i.e. the dominant feature at the interface is a discontinuity in a finite constant viscosity between the two fluids), and we should therefore expect similar behaviour with respect to the short wavelength instabilities as for 2 Newtonian fluids. Long wavelength instabilities can be analysed by using regular perturbation methods, from the linearised stability equations for each generalised Newtonian fluid, (e.g. as in [19]). This methodology is analogous to that used in the Newtonian fluid studies and hence the qualitative similarity is not surprising. Pinarbasi and Liakopoulos [21] have considered the stability of a two-layer Poiseuille flow of both CarreauYasuda and Bingham-like fluids. However, Pinarbasi and Liakopoulos do not model a true Bingham fluid (i.e. with a yield stress). Instead, they choose a form of regularised viscosity model in which the effective viscosity attains a Newtonian limit at zero shear-rate. This modified constitutive model is therefore qualitatively similar to the CarreauYasuda model that is also studied in [21].

Multi-layer viscoelastic flows have been studied by ...

In this paper we study multi-layer flows that are linearly stable even at infinite Re. In view of the above results, this may seem unlikely. However, or approach is straightforward. First we eliminate interfacial instabil-

ities by ensuring that for the base flow configurations studied we maintain an unyielded plug region at the interface. Secondly we eliminate linear shear instabilities by ensuring a strong enough Couette component in the lubricated fluid layer. The fluids that we consider are a lubricating layer of a yield stress fluid (for simplicity a Bingham fluid), adjacent to a lubricated layer of either a Carreau fluid or a **m**odified **C**hilcott-**R**allison FENE fluid (MCR fluid).

Elimination of interfacial instabilities via the presence of an unyielded plug was first studied by Frigaard [25], who studied a linear stability problem involving two Bingham fluids. The main idea is that in a Poiseuille-like configuration the stress at the interface will be a finite amount below the yield stress. In consequence an infinitesimal disturbance cannot cause the fluid to yield and therefore the interface is not deformed. The base linear stability of such flows is therefore determined by the underlying shear flow instability, not by interfacial modes, and such flows may indeed be more stable than the corresponding single fluid flow. In [2] it was shown that this interfacial stability in fact carries over to bounded nonlinear perturbations and in [3] these stable multi-layer flows were demonstrated experimentally. This flow methodology has been termed visco-plastic lubrication.

Elimination of shear instabilities via introduction of a Couette component was first studied by [28,29], who considered plane Couette-Poiseuille (PCP) flows. Plane Poiseuille flow becomes unstable at $Re \approx 5772$, [9], whereas plane Couette flow is linearly stable at $Re = \infty$, [10]. Potter [28] and Hains [29] showed that for a sufficiently strong Couette component PCP flows would also become stable at $Re = \infty$, i.e. when the lower wall velocity exceeded a critical cut-off value, approximately equal to 0.7 times the maximal velocity of the plane Poiseuille flow. The mechanism of stability was further elucidated by [30] who studied a long wave limit to compute the cut-off velocity.

PCP flows of both Carreau fluids and of MCR fluids have been studied by the authors in [31,27]. In both cases we have shown that the same cut-off mechanism is present for these non-Newtonian fluids and may be computed via the long wavelength limit of [30]. The plan of the paper therefore is to combine the methodology of visco-plastic lubrication with the stabilising effects of a strong Couette component. Below, in section 2 we describe the underlying base flows that we study. Section 3 presents the linear stability problems and results of our analysis. The paper concludes with a length discussion in 4.

2 Problem statement

The 2D flow geometry we consider is described in Fig. 1. Two fluids of identical density $\hat{\rho}$ flow in a plane channel, oriented with the $\hat{x}$-axis. The interface position of the base flow is used to fix the $\hat{y}$-axis, at $\hat{y} = 0$. The upper fluid occupies the region between the interface and the upper wall at $\hat{y} = \hat{h}$, while the lower fluid occupies the
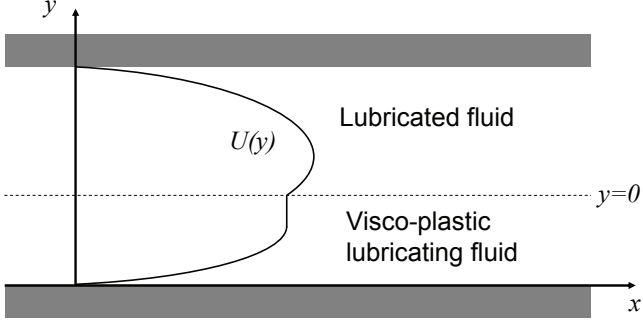
Fig. 1 Schematic of the flow geometry.

region between the interface and the lower wall at $\hat{y} = -\hat{a}$. The flow is driven by an imposed constant axial pressure gradient, $(-\mathrm{d}\hat{p}/\mathrm{d}\hat{x}, 0,)$.

The upper fluid will be either shear-thinning or visco-elastic. For definiteness and to take advantage of previous results, we consider either a Carreau fluid or a modified FENE Chilcott-Rallison fluid, (MCR fluid). The lower fluid has a yield stress, and for simplicity we select the classical Bingham fluid model. We do not believe that the essence of our results changes much if other similar fluid models are chosen. As explained in Sect. 1, our objective is to observe how the yield stress fluid layer may enhance the flow of the upper fluid, both in terms of increasing the volumetric flux of the upper fluid and in improving the (linear) stability. Therefore conceptually, we base our scaling on the pressure driven flow of the upper fluid, traveling alone in a plane channel of width $\hat{h}$.

Throughout this paper we adopt the convention of denoting dimensional variable with a $\hat{}$ symbol and di-

mensionless variables without. We make the equations of motion dimensionless by using $\hat{h}$ as length-scale, $\hat{U}_{max}$ as velocity-scale, $\hat{h}/\hat{U}_{max}$ as timescale, $\hat{\rho}\hat{U}_{max}^2$ as pressure scale, and $\hat{\mu}_0\hat{U}_{max}/\hat{h}$ as viscous and elastic stress scale. The velocity $\hat{U}_{max}$ is defined to be the maximal (centreline) velocity of the upper fluid, traveling alone in a plane channel of width $\hat{h}$, driven by the pressure gradient $(-\mathrm{d}\hat{p}/\mathrm{d}\hat{x}, 0,)$. The viscosity $\hat{\mu}_0$ is either the low shear viscosity of the Carreau fluid or the total viscosity of the MCR fluid, as discussed below. As we do not combine these models, no confusion need arise. With these scalings, the equations of motion in the lower and upper fluid layers are as follows.

2.0.1 Lower fluid layer, $y \in (-a, 0)$ In the Bingham fluid the following dimensionless equations are satisfied

$$\nabla \cdot \boldsymbol{u} = 0, \tag{1}$$

$$\frac{\partial \boldsymbol{u}}{\partial t} + (\boldsymbol{u} \cdot \nabla)\boldsymbol{u} = -\nabla p + \frac{m}{Re}\nabla \cdot \boldsymbol{\tau}_B, \tag{2}$$

The modified pressure and the deviatoric stress tensor are denoted p and $\boldsymbol{\tau}_B = \tau_{B,ij}$, respectively. The two dimensionless parameters appearing above are the Reynolds number Re and the viscosity ratio m. These are defined as follows:

$$Re \equiv \frac{\hat{\rho}\hat{U}_{max}\hat{h}}{\hat{\mu}_0}, \qquad m \equiv \frac{\hat{\mu}_p}{\hat{\mu}_0}, \tag{3}$$

where $\hat{\mu}_p$ is the plastic viscosity of the Bingham fluid.

The Bingham fluid is described by the following scaled constitutive laws:

$$\dot{\gamma}(\boldsymbol{u}) = 0 \iff \tau_B(\boldsymbol{u}) \leq B, \quad (4)$$

$$\tau_{B,ij}(\boldsymbol{u}) = \left[1 + \frac{B}{\dot{\gamma}(\boldsymbol{u})}\right] \dot{\gamma}_{ij}(\boldsymbol{u}) \iff \tau_B(\boldsymbol{u}) > B. \quad (5)$$

The 3rd dimensionless parameter appearing above is the Bingham number B:

$$B \equiv \frac{\hat{\tau}_Y \hat{h}}{\hat{\mu}_p \hat{U}_{max}}, \quad (6)$$

where $\hat{\tau}_Y$ is the yield stress of the lubricating fluid. Physically, B is the ratio of yields stress to viscous stress, but also represents the dimensionless yield stress of the fluid. The rate of strain and deviatoric stress second invariants, $\dot{\gamma}$ and τ_B respectively, are defined by:

$$\dot{\gamma} = \left[\frac{1}{2} \sum_{i,j=1}^{2} [\dot{\gamma}_{ij}]^2\right]^{1/2} \qquad \tau_B = \left[\frac{1}{2} \sum_{i,j=1}^{2} [\tau_{B,ij}]^2\right]^{1/2}$$

where $x \equiv x_1$, $y \equiv x_2$, $u \equiv u_1$, $v \equiv u_2$ and

$$\dot{\gamma}_{ij} = \frac{\partial u_i}{\partial x_j} + \frac{\partial u_j}{\partial x_i}, \qquad i,j = 1,2. \quad (7)$$

2.0.2 Upper layer, $y \in (0,1)$: MCR fluid In the case that the upper layer contains an MCR fluid, (1) is satisfied, coupled with

$$\frac{\partial \boldsymbol{u}}{\partial t} + (\boldsymbol{u} \cdot \boldsymbol{\nabla})\boldsymbol{u} = -\nabla p + \frac{\beta}{Re} \boldsymbol{\nabla} \cdot \dot{\boldsymbol{\gamma}} + \frac{1}{Re} \boldsymbol{\nabla} \cdot \boldsymbol{\tau} \quad (8)$$

where β denotes the solvent to total viscosity ratio and Re is defined via (3), using the total viscosity of the MCR fluid, $\hat{\mu}_0$. The constitutive equation for the elastic stress tensor $\boldsymbol{\tau}$ is:

$$\boldsymbol{\tau} + \frac{We}{f(\boldsymbol{\tau})} \overset{\triangledown}{\boldsymbol{\tau}} = (1-\beta)\dot{\boldsymbol{\gamma}} \quad (9)$$

where $f(\boldsymbol{\tau})$ describes the spring law. The function $f(\boldsymbol{\tau})$ is given by

$$f(\boldsymbol{\tau}) = \frac{b + \frac{We}{(1-\beta)} \text{tr}\boldsymbol{\tau}}{b-d}. \quad (10)$$

Here "tr" is the trace operator, We is the Weissenberg number which is the ratio of a relaxation timescale of the fluid, say $\hat{t}_r$, to the advective timescale of the flow, $\hat{h}/\hat{U}_{max}$, and b is the extensibility parameter that measures the size of the polymer molecule in relation to its equilibrium size. Values for b used in the literature are in the range of 10^2 to 10^3 and following the work of Remmelgas et al. [22], we take as a base value, $b = 100$. The dimensionless parameter b is often denoted L^2 in the literature. Note that we recover the Oldroyd-B model as a special case if we take $b \to \infty$, when $f(\boldsymbol{\tau}) \to 1$. The parameter d is the dimension of the configuration space. For brevity, we refer to [23] for a discussion of these parameters in a more general context. Later when we consider the high Re limit of these flow, in place of We we shall use the alternative dimensionless elasticity parameter, $\epsilon = We/Re$, which is the ratio of kinematic viscosity and relaxational diffusivity. Note that ϵ depends on the properties of the fluid and the flow geometry, but not the velocity scale. In the case of an MCR fluid, the velocity scale is simply:

$$\hat{U}_{max} = \frac{-\text{d}\hat{p}/\text{d}\hat{x}}{8\hat{\mu}_0\hat{h}^2}. \quad (11)$$

2.0.3 Upper layer, $y \in (0,1)$: Carreau fluid In the case that the upper layer contains a Carreau fluid, (1) is sat-

isfied, coupled with

$$\frac{\partial \boldsymbol{u}}{\partial t} + (\boldsymbol{u} \cdot \nabla)\boldsymbol{u} = -\nabla p + \frac{1}{Re}\nabla \cdot \boldsymbol{\tau}_C, \qquad (12)$$

The deviatoric stress $\boldsymbol{\tau}_C$ satisfies the constitutive equation

$$\boldsymbol{\tau}_C = \left(\mu_\infty + [1 - \mu_\infty]\left[1 + (\lambda\dot{\gamma})^2\right]^{(n-1)/2}\right)\dot{\boldsymbol{\gamma}}. \quad (13)$$

The Reynolds number Re is as defined in (3), using the low shear Carreau viscosity $\hat{\mu}_0$. The other rheological parameters are $\mu_\infty = \hat{\mu}_\infty/\hat{\mu}_0$, denoting the ratio of high to low shear viscosities, (typically $\mu_\infty < 1$), the dimensionless power-law index $n \leq 1$, and $\lambda = \hat{\lambda}\hat{U}_0/\hat{h}$. Here $\hat{\lambda}$ is the dimensional time constant of the Carreau model and $1/\hat{\lambda}$ is indicative of the dimensional rate of strain at which shear-thinning effects become significant. Thus, λ is the ratio of this strain rate to a representative strain rate of the flow. It is a combination of n and λ that govern the degree of shear-thinning. Note that the Newtonian fluid is recovered in any of the limits: $\lambda = 0$, $n = 1$ or $\mu_\infty = 1$.

The velocity scale $\hat{U}_{max}$ needs to be found from a plane channel Poiseuille flow problem, which is straightforward to solve. Dispensing with the details, we find that

$$\hat{U}_{max} = \frac{1}{g}\frac{-\mathrm{d}\hat{p}/\mathrm{d}\hat{x}}{\hat{\mu}_0 \hat{h}^2} : \quad g = \int_0^{g/2} \dot{\gamma}(\tau)\,\mathrm{d}\tau. \qquad (14)$$

The function $\dot{\gamma}(\tau)$ is found by inverting the constitutive law, i.e.

$$\tau = \left(\mu_\infty + [1 - \mu_\infty]\left[1 + (\lambda\dot{\gamma})^2\right]^{(n-1)/2}\right)\dot{\gamma},$$

a)

b)
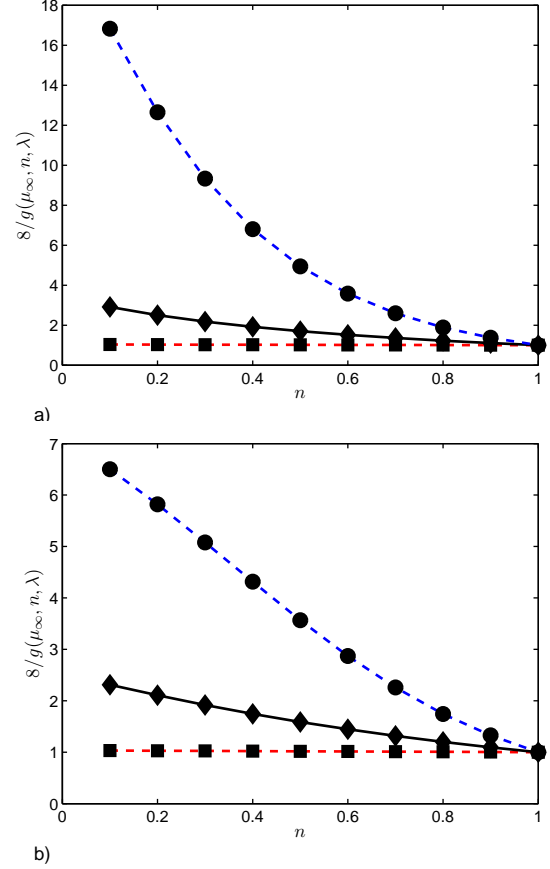
Fig. 2 The function $8/g(\mu_\infty, n, \lambda)$: a) $\mu_\infty = 0.01$; b) $\mu_\infty = 0.1$. In each figure: $\lambda = 0.1 - \blacksquare$, $\lambda = 1 - \blacklozenge$, $\lambda = 10 - \bullet$.

and g is found iteratively using any simple numerical solver. Since the constitutive law depends upon the dimensionless groups (μ_∞, n, λ), it is evident that $g = g(\mu_\infty, n, \lambda)$. In any of the Newtonian limits of the Carreau model, $\dot{\gamma}(\tau) = \tau$, leading to $g = 8$. Figure 2 explores the variation of $8/g(\mu_\infty, n, \lambda)$, which indicates the ratio of $\hat{U}_{max}$ for the Carreau fluid to $\hat{U}_{max}$ for a Newtonian fluid with equal low shear viscosity. We observe that this ratio increases significantly for large λ and small n, for which shear-thinning effects are prevalent.

2.1 Boundary and interfacial conditions

The interface of the base flow has been positioned at $y = 0$. In the case that the flow is unsteady, the interface position will be denoted $y = y_i(x, t)$ and is governed by the kinematic equation:

$$\frac{\partial y_i}{\partial t} + u \frac{\partial y_i}{\partial x} = v. \qquad (15)$$

Across the interface both the velocity and traction vectors are continuous. At the solid walls of the flow, no slip boundary conditions are satisfied.

2.2 Base flows

Before computing the base flows directly, we may consider some general features. First of all, considering the full channel, $y \in [-a, 1]$, it is evident that the base velocity $U(y)$ is Poiseuille like, i.e. the shear stress increases linearly with distance from the lower wall, and must be zero somewhere in the interior; also there will be a single maximum value of $U(y)$. Secondly, considering only the lower Bingham fluid layer and the linear increase of shear stress, we may have one of 4 possibilities: (1) the interfacial stress is below the yield stress but the stress at the lower wall exceeds the yield stress; (2) the interfacial stress is below the yield stress and the stress at the lower wall is also below the yield stress; (3) the magnitude of the interfacial stress is above the yield stress and the interfacial stress is positive; (4) the magnitude of the interfacial stress is above the yield stress and the
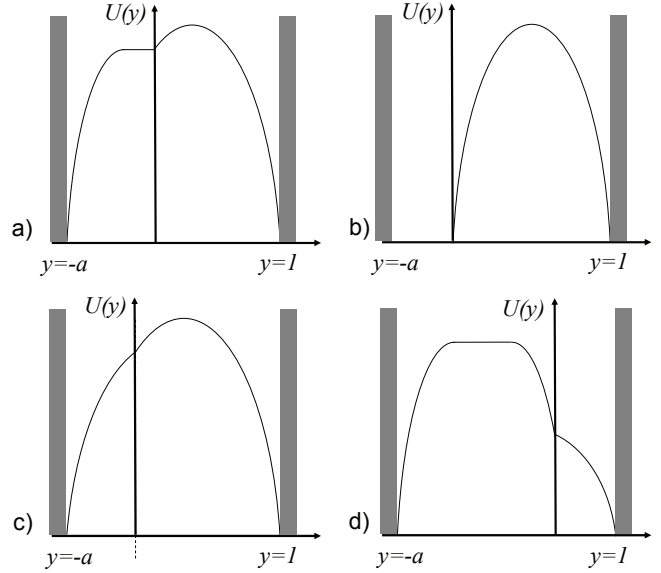
Fig. 3 Different types of base solution: a) type 1; b) type 2; c) type 3; d) type 4.

interfacial stress is negative. Schematically, the base velocity profiles corresponding to (1)-(4) are as illustrated in Fig. 3. We refer to these as solutions of types 1-4, and will only be interested in solutions of type 1.

2.2.1 Bingham fluid & MCR fluid
For the MCR fluid in the upper layer, the base solution satisfies the following 1D system:

$$-8 = m \frac{\mathrm{d}}{\mathrm{d}y} \tau_{B,xy}, \qquad y \in (-a, 0), \qquad (16)$$

$$-8 = U''(y), \qquad y \in (0, 1), \qquad (17)$$

$$U(y) = 0, \quad \text{at} \quad y = -a, \ 1, \qquad (18)$$

$$U(0^+) = U(0^-), \qquad (19)$$

$$U'(0^+) = m \tau_{B,xy}(0^-), \qquad (20)$$

where

$$|U'(y)| = 0 \iff |\tau_{B,xy}| \leq B, \quad (21)$$

$$\tau_{B,xy} = \left[1 + \frac{B}{|U'(y)|}\right] U'(y) \iff |\tau_{B,xy}| > B. \quad (22)$$

This system can be solved analytically for the 4 different types of solution, but the reader is spared the details of these lengthy calculations.

We may note that $U(y)$, depends only on (m, B, a). Our interest is exclusively in the type 1 solutions, which may be found in a region of the positive $(a, mB/4)$-plane, defined by the following bounds:

$$a \geq \frac{1}{2}\left[\frac{mB}{4} - 1\right], \qquad \text{Type 1-2,} \tag{23}$$

$$a \geq m^{1/2}\left[1 - \frac{mB}{4}\right]^{1/2}, \qquad \text{Type 1-3,} \tag{24}$$

$$a \leq \frac{mB}{4} + m^{1/2}\left[1 + \frac{mB}{4}\right]^{1/2}, \qquad \text{Type 1-4,} \tag{25}$$

as illustrated in Fig. 4 for various m. We should note that although this region is unbounded in a, for an application in which the lower fluid layer is used as a lubricant, large a implies an increasing consumption of lubricant so that practical bounds will exist.

For each type 1 solution, the thickness of the plug region is denoted y_p, which may be found as the solution of the quadratic:

$$\frac{4}{m}(a - y_p)^2 = 4 - mB + 8y_p.$$

Having found y_p, the interfacial shear stress is denoted by: $\tau_i = mB - 8y_p$, and the velocity at the interface is denoted $U_0 = 4 - \tau_i$. For completeness, the velocity profiles in the two layers are:

$$U(y) = \begin{cases} U_0 \dfrac{(a+y)(a-y-2y_p)}{(a-y_p)^2} & y \in [-a, -y_p], \\ U_0 & y \in (-y_p, 0], \\ U_0(1-y) + 4y(1-y), & y \in (0, 1], \end{cases}$$
$$\tag{26}$$
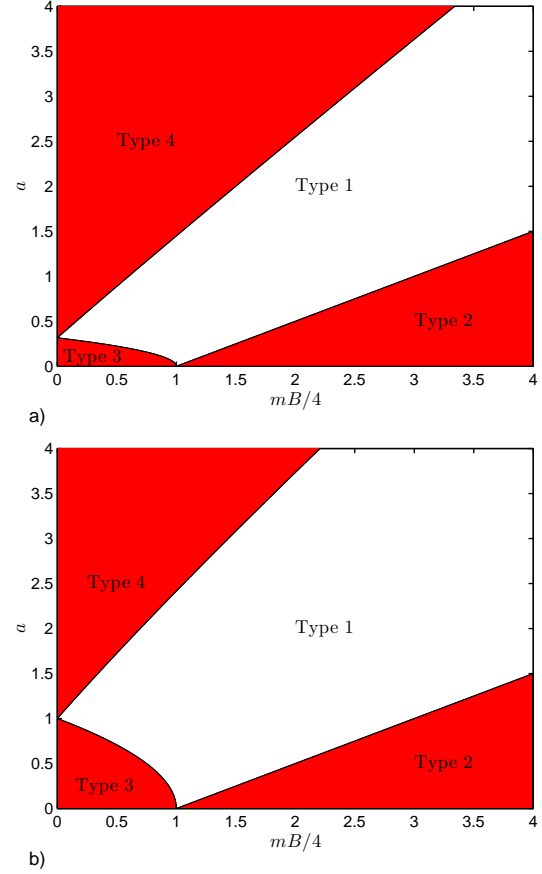
Fig. 4 Regimes for the solution types: a) $m = 0.1$; b) $m = 1$.

and the dimensionless pressure gradient is simply $P'(x) = -8/Re$. The elastic stresses of the base flow are denoted T_{ij} and are found in terms of $U(y)$:

$$T_{xx} = \Lambda(U'(y); We, \beta, b, d), \tag{27}$$

$$T_{xy} = (1 - \beta)U'(y), \tag{28}$$

$$T_{yy} = 0, \tag{29}$$

where Λ is the positive root of

$$\Lambda^2 + \frac{b(1-\beta)}{We}\Lambda - 2(1-\beta)(b-d)[U'(y)]^2 = 0.$$

From the form of (26) we can see that the areal flux in the MCR layer is increased from $1/2$ to $(1+U_0)/2$ by the lubricating layer. The form of the velocity solution in the upper layer divides into the original Poiseuille

component, i.e. in the absence of the lower layer, and what might be termed a Couette component, due to the moving interface. It is the Couette contribution that increases the flux. We may also calculate the flux of lubricant straightforwardly.

2.2.2 Bingham fluid & Carreau fluid   With the Carreau fluid in the upper layer, the base solution satisfies the following 1D system:

$$-g = m\frac{\mathrm{d}}{\mathrm{d}y}\tau_{B,xy}, \qquad y \in (-a, 0), \qquad (30)$$

$$-g = \frac{\mathrm{d}}{\mathrm{d}y}\tau_{C,xy}, \qquad y \in (0, 1), \qquad (31)$$

$$U(y) = 0, \quad \text{at} \quad y = -a,\ 1, \qquad (32)$$

$$U(0^+) = U(0^-), \qquad (33)$$

$$\tau_{C,xy}(0^+) = m\tau_{B,xy}(0^-), \qquad (34)$$

where

$$\tau_{C,xy} = \left(\mu_\infty + [1 - \mu_\infty]\left[1 + (\lambda|U(y)|)^2\right]^{(n-1)/2}\right)U(y). \qquad (35)$$

We recall that $g = g(\mu_\infty, n, \lambda)$. It is not possible to solve analytically for the base flow, except in the limiting cases for which the Carreau fluid is Newtonian. However, numerical integration is straightforward.

For any fixed (μ_∞, n, λ) the parameter region in which type 1 solutions are found can be determined and plotted in the plane $(a, 2mB/g)$, as we illustrate in Fig. 5. The bounds of the regions in Fig. 5 may be determined

semi-analytically, and are given by:

$$a \geq \frac{1}{2}\left[\frac{2mB}{g} - 1\right], \qquad \text{Type 1-2,} \qquad (36)$$

$$a \geq \left[\frac{2m}{g}U_{0,C}(\mu_\infty, n, \lambda, mB)\right]^{1/2}, \qquad \text{Type 1-3,} \qquad (37)$$

$$a \leq \frac{2mB}{g} + \left[\frac{2m}{g}U_{0,C}(\mu_\infty, n, \lambda, -mB)\right]^{1/2}, \qquad \text{Type 1-4,} \qquad (38)$$

where $U_{0,C}(\mu_\infty, n, \lambda, \tau_i)$ is the velocity at $y = 0$ obtained by solving (31) with $\tau_{C,xy} = \tau_i$ at $y = 0$ and $U(y) = 0$ at $y = 1$. We observe that the location of the different solution type regions are qualitatively similar to those of the Bingham-MCR pairing. In general terms, we find that increasing the shear-thinning characteristics of the Carreau fluid layer tends to increase the region of Type 1 flows, as viewed in terms of $(a, 2mB/g)$. Note that in the absence of the lubricating layer, $g/2$ would denote the shear stress at $y = 0$. Thus, the significance of the quantity $2mB/g$ is the ratio of the yield stress to the wall shear stress in the absence of lubrication.

3 Linear stability

We now consider a linear perturbation of multi-layer type 1 flow. We proceed in the usual fashion, assuming an x-periodic modal disturbance to the base flow and using domain perturbation for both the yield surface, in the Bingham fluid layer, and the interface.

Type 1 base flows are characterised by an unyielded plug region of width y_p, lying in $[-y_p, 0]$. The plug width y_p vanishes only at the boundary with the type 3 velocity
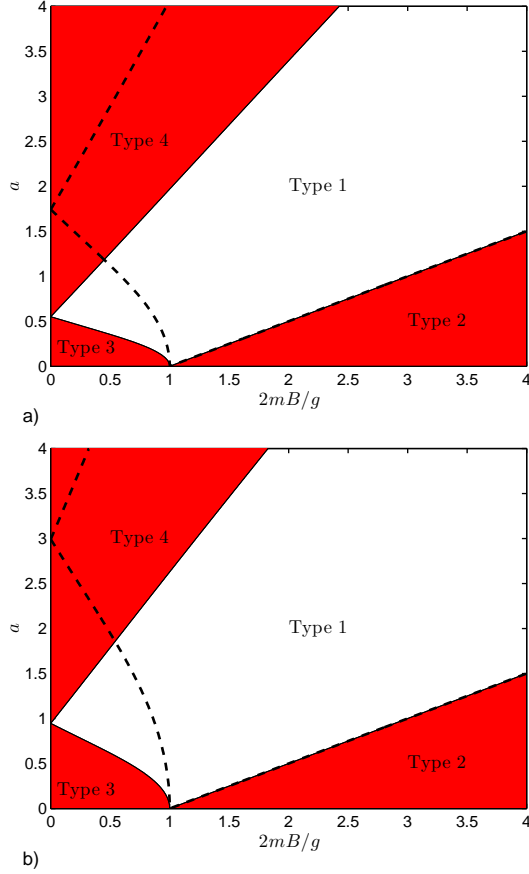
Fig. 5 Regimes for the solution types: a) $(\mu_\infty, n, \lambda) = (0.01, 0.5, 1)$; b) $(\mu_\infty, n, \lambda) = (0.01, 0.5, 10)$. In both figures $m = 0.1$ is marked with the shaded regions and the dashed lines mark the shift in the region boundaries for $m = 1$.

region, but is otherwise of finite width. The yield stress is attained at $y = -y_p$, and consequently the interfacial stress τ_i is always a finite amount below the yield value mB whenever y_p is finite. In contrast the stress and velocity perturbations are infinitesimal in a linear stability analysis. It follows that for a type 1 flow (or indeed also a type 2 flow), the linear perturbation is unable to exceed the yield stress at the interface. Consequently the interface remains undeformed.

A careful analysis of the yield surface perturbation and plug motion follows that in e.g. [24,25]. the conclu-

sion of this analysis is that although a modal perturbation of the yield surface occurs, the plug itself is not moved by the perturbation. The reason for this is that the modal stresses are periodic in the x-direction and thus the net traction on the plug over one period is zero. The perturbations with zero wavenumber may be shown to be stable. The key consequence of this feature, unique to yield stress fluids in such configurations, is that the linear stability eigenvalue problems for the different fluid regions decouple, linked only by the parameters of the base flow.

For 2 dimensional perturbations, we introduce a stream function and cross differentiate to eliminate the pressure. The resulting eigenvalue problem in the yielded Bingham fluid region, $y = \in (-a, -y_p)$, is:

$$i\alpha c(\alpha^2 - D^2)\phi = \frac{m}{Re}\left[(\alpha^2 - D^2)^2\phi - 4\alpha^2 BD\left(\frac{D\phi}{|DU|}\right)\right]$$
$$+ i\alpha[D^2U + U(\alpha^2 - D^2)]\phi. \quad (39)$$

$$\phi = D\phi = 0, \quad \text{at } y = -a, \; -y_p, \quad (40)$$

$$y'_p = -\frac{D^2\phi(-y_p^-)}{D^2U(-y_p^-)} \quad (41)$$

Here $D = \frac{d}{dy}$. The linear perturbations of the velocity (u', v') are related to the stream function Ψ by $u' = \Psi_y$, $v' = -\Psi_x$, and the modal form of perturbation is then:

$$\Psi \sim \phi(y)e^{i\alpha(x-ct)}. \quad (42)$$

The yield surface perturbation is $y'_p e^{i\alpha(x-ct)}$.

If the upper layer contains an MCR fluid, the modal form of the elastic stress perturbation is $\tau_{ij}(y)e^{i\alpha(x-ct)}$,

$ij = xx,\ xy,\ yx,\ yy$, and eigenvalue problem for $y \in (0,1)$ is:

$$i\alpha c(\alpha^2 - D^2)\phi = i\alpha[D^2U + U(\alpha^2 - D^2)]\phi$$
$$+ \frac{1}{Re}[i\alpha(\tau_{xx} - \tau_{yy}) + (D^2 + \alpha^2)\tau_{xy}]$$
$$+ \frac{\beta}{Re}(\alpha^2 - D^2)^2\phi \qquad (43)$$

$$i\alpha c F(y)\tau_{xx} = \left[1 + i\alpha F(y)U + \frac{F(y)T_{xx}}{(1-\beta)(b-d)}\right]\tau_{xx}$$
$$- 2F(y)DU\tau_{xy} + \frac{F(y)T_{xx}}{(1-\beta)(b-d)}\tau_{yy}$$
$$- i\alpha F(y)DT_{xx}\phi - 2F(y)T_{xy}D^2\phi$$
$$- 2i\alpha\left[F(y)T_{xx} + (1-\beta)\right]D\phi \qquad (44)$$

$$i\alpha c F(y)\tau_{xy} = [1 + i\alpha F(y)U]\,\tau_{xy} - F(y)DU\tau_{yy}$$
$$- (1-\beta)D^2\phi - \alpha^2(1-\beta)\phi$$
$$- \left[i\alpha F(y)DT_{xy} + F(y)\alpha^2 T_{xx}\right]\phi \qquad (45)$$

$$i\alpha c F(y)\tau_{yy} = 2i\alpha(1-\beta)D\phi - 2F(y)\alpha^2 T_{xy}\phi$$
$$+ [1 + i\alpha F(y)U]\,\tau_{yy}. \qquad (46)$$

with boundary conditions:

$$\phi = D\phi = 0, \quad \text{at } y = 0, 1. \qquad (47)$$

The function $F(y)$ is:

$$F(y) = \frac{We(b-d)}{b + WeT_{xx}/(1-\beta)}. \qquad (48)$$

Finally, if instead the upper layer contains a Carreau fluid, the eigenvalue problem for $y \in (0,1)$ is:

$$i\alpha c\left(\alpha^2 - D^2\right)\phi = i\alpha\left[U\left(\alpha^2 - D^2\right) + D^2 U_b\right]$$
$$+ \frac{1}{Re}\left(D^2 + \alpha^2\right)\left[\mu_t\left(D^2 + \alpha^2\right)\phi\right]$$
$$- \frac{4\alpha^2}{Re}D\left(\mu D\phi\right). \qquad (49)$$

with

$$\phi = D\phi = 0 \ \text{ at } \ y = 0 \text{ and } y = 1, \qquad (50)$$

and where μ and μ_t are respectively the effective viscosity and tangent viscosity, for the Carreau fluid:

$$\mu(\dot\gamma) = \left(\mu_\infty + [1 - \mu_\infty]\left[1 + (\lambda\dot\gamma)^2\right]^{(n-1)/2}\right) \qquad (51)$$
$$\mu_t(\dot\gamma) = \mu(\dot\gamma) + \frac{d\mu}{d\dot\gamma}. \qquad (52)$$

These are evaluated at $\dot\gamma = |DU|$.

3.1 Stability of the Bingham layer

On introducing the mapping $y = -y_p - \xi(a - y_p)$, $c = U_0\tilde c$, $U = U_0\tilde U(U)(\xi) = U_0(1 - \xi^2)$, $\tilde\alpha = \alpha(a - y_p)$, $\tilde{Re} = ReU_0(a - y_p)/m$, $\tilde B = BU_0(a - y_p)$, $\tilde y_p = y_p'U_0$, this eigenvalue problem assumes the following standard form for $\xi \in (0,1)$:

$$i\tilde\alpha\tilde c(\tilde\alpha^2 - \tilde D^2)\phi = \frac{1}{\tilde{Re}}\left[(\tilde\alpha^2 - \tilde D^2)^2\phi - 4\tilde\alpha^2\tilde B\tilde D\left(\frac{\tilde D\phi}{|\tilde D\tilde U|}\right)\right]$$
$$+ i\tilde\alpha[\tilde D^2\tilde U + \tilde U(\tilde\alpha^2 - \tilde D^2)]\phi, \qquad (53)$$

$$\phi = \tilde D\phi = 0, \quad \text{at } \xi = 0,\ 1, \qquad (54)$$

$$\tilde y_p = -\frac{\tilde D^2\phi(0^+)}{\tilde D^2\tilde U(0^+)}, \qquad (55)$$

where $\tilde D = \frac{d}{d\xi}$.

This eigenvalue problem is precisely that derived by [24] for plane channel flow of a Bingham fluid and the mapping used is similar to that in [25]. In [24] the authors analysed the even extensions of the above eigenvalue problem, in fact replacing the above boundary conditions at $\xi = 0$ with $D\phi = D^3\phi = 0$. In this way they were able to compute marginal stability results that vary continuously from the Newtonian results as $\tilde B$ is increased from zero. However, splitting into odd and even components is not justified here.

Instead, with the conditions $\phi = \tilde{D}\phi = 0$, no unstable modes have ever been found. This case has been extensively studied by [26] and although there is no analytical proof of the unconditional linear stability, the arguments are strong. In particular, in examining the spectra of (53)-(55) the Bingham fluid term is observed to have a stabilising effect. If one sets $\tilde{B} = 0$ we recover the Newtonian Orr-Somerfeld problem for a plane channel Couette-Poiseuille flow, in which the wall velocity matches with the maximal velocity of the channel. This case is known to be stable for all $\tilde{Re}$ and on this basis we infer that the Bingham fluid layer is also linearly stable for all $\tilde{Re}$.

Table 1 Cut-off velocity values U_0 for different ϵ and extensibility b; from [27].

ϵ	$b = 100$	$b = 1000$	$b = 10000$	$b = \infty$
2×10^{-8}	0.7095	0.7095	0.7095	0.7095
2×10^{-7}	0.7104	0.7103	0.7109	0.7108
4×10^{-7}	0.7112	0.7112	0.7118	0.7121
10^{-6}	0.7110	0.7144	0.7154	0.7143

3.2 Results: stability of the MCR layer

The eigenvalue problem (43)-(48) is identical to that studied by the authors in [27], with "lower wall velocity" V in [27] replaced by the interfacial velocity U_0 here (for type I flows). For both fixed We and fixed elasticity number $\epsilon = We/Re$ it was shown that as U_0 increases significantly from zero, the stability increases and the branches of the marginal stability curve in the (Re, α) become parallel with lines $Re \sim \alpha^{-1}$ as $Re \to \infty$. This picture qualitatively follows that for a Newtonian plane Couette-Poiseuille (PCP) flow, as studied by [28–30].

The observed behaviour along the branches of the marginal stability curves prompts consideration of the long-wave limit of [30], in which $\alpha \to 0$ with $Re\alpha$ fixed. This distinguished limit leads to a simplified eigenvalue problem for which it is found that there are no unstable eigenvalues with U_0 above a certain "cut-off" value, i.e. essentially when the Couette component becomes strong enough. In [30] this cut-off value is determined for Newtonian fluids to be $U_0 \approx 0.7$. In [27] we have considered the same limit for MCR fluids. Surprisingly, for both fixed We and fixed ϵ, this distinguished limit is identical to that for Newtonian fluids. This cut-off value is also computed directly from (43)-(48) in [27] (see Table 1) and this confirms numerically that the cut-off limit is independent of the elastic parameters of the flow.

We now observe that for any parameters m, a, B, such that the base flow is of type I, we may compute the interfacial velocity U_0. If we find that, for example conservatively, $U_0 > 0.72$, then it appears that the MCR
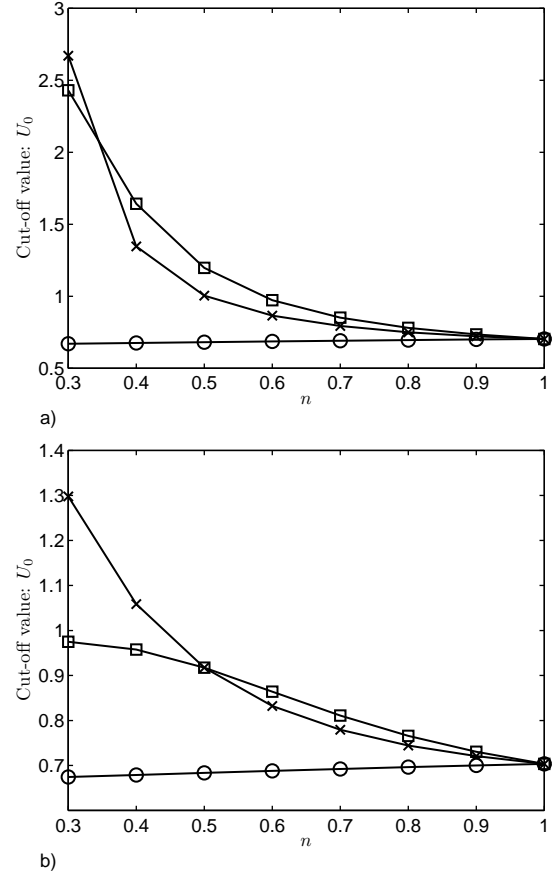
a)

b)
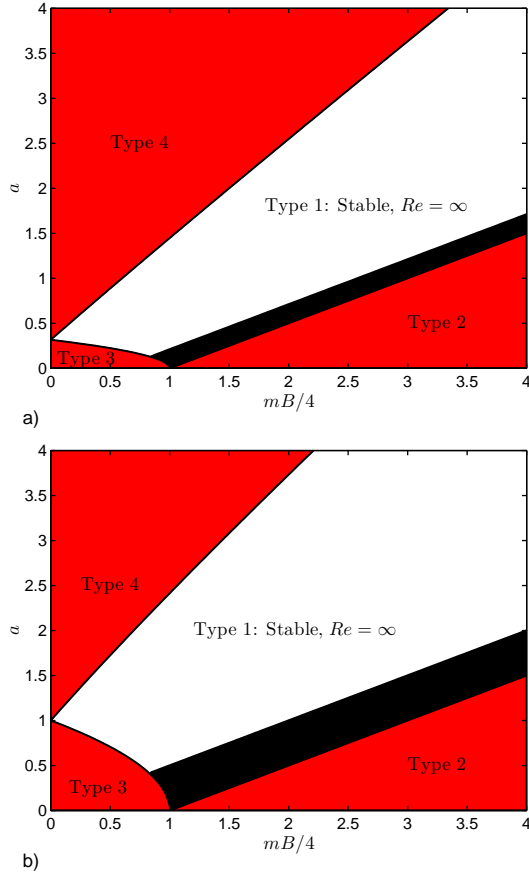
Fig. 6 Regimes where the multi-layer Bingham-MCR flow is linearly stable for all Re: a) $m = 0.1$; b) $m = 1$.

a)

b)

Fig. 7 Cut-off values of U_0, above which the Carreau PCP flow is linearly stable for all Re, from [31]: a) $\mu_\infty = 0.01$; b) $\mu_\infty = 0.1$. In each plot: $\lambda = 0.1$ (○); $\lambda = 1$ (×); $\lambda = 10$ (□).

fluid layer is linearly stable for all Re. Since the Bingham fluid layer is also stable for all Re, multi-layer flows for these parameters are linearly stable for all Re. With reference to Fig. 4, the boundary between type I and type II solutions is characterised by $U_0 = 0$. Thus, the region of linearly stable flows at all Re is located away from this boundary.

3.3 Results: stability of the Carreau layer

As in the previous section, for a type I solution the Carreau fluid layer eigenvalue problem (49) & (50) has been studied by the authors in [31], for a PCP flow. Qualitatively the results are as for the Newtonian fluid, with

the cut off velocity determined by the longwave distinguished limit, $\alpha \to 0$ with $Re\alpha$ fixed. The only difference is that the cut off values of U_0 vary significantly with (μ_∞, n, λ), as shown below in Fig. 7. Samples of parameter regions that are linearly stable at all Re are shown in Fig. 8.

4 Discussion

In this paper we have shown that it is possible to achieve multi-layer parallel flows that are stable at $Re = \infty$ for a wide range of fluids, including both shear-thinning and
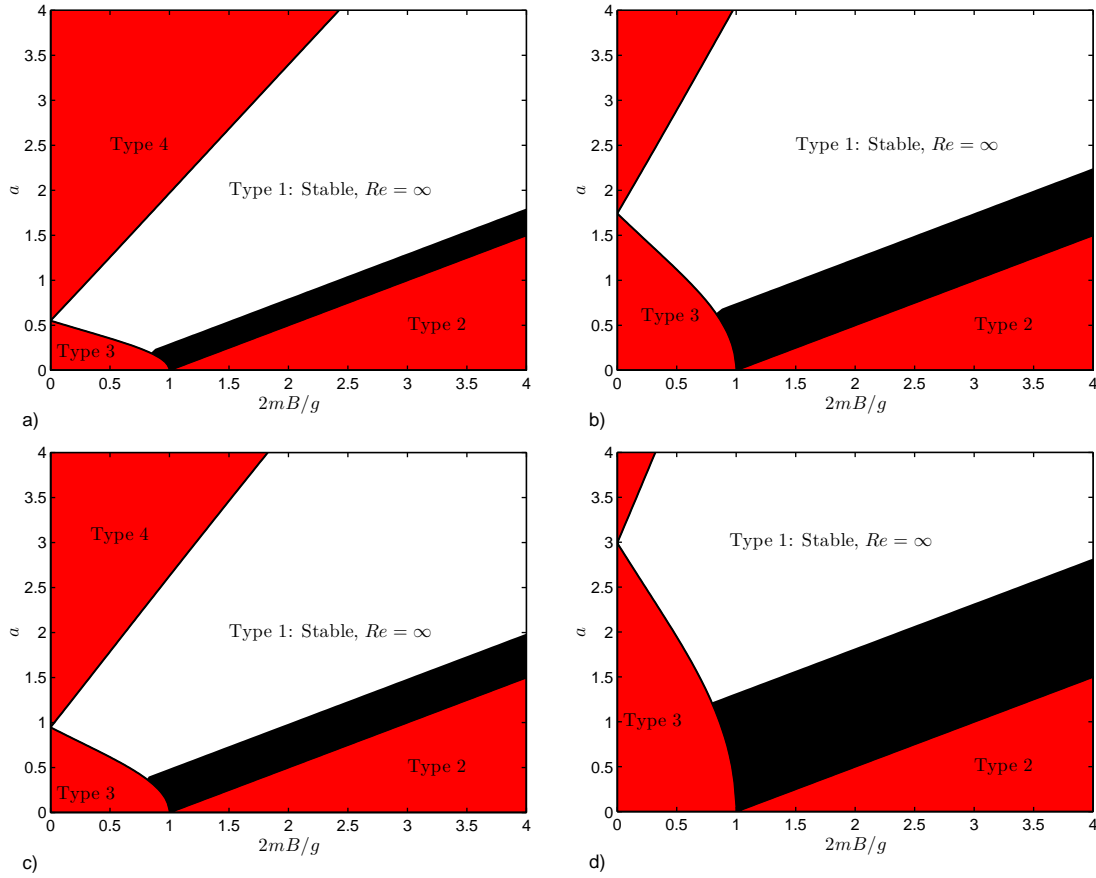
Fig. 8 Regimes where the multi-layer Bingham-Carreau flow is linearly stable for all Re: $(\mu_\infty, n) = (0.01, 0.5)$, a) $\lambda = 1$, $m = 0.1$; b) $\lambda = 1$, $m = 1$; c) $\lambda = 10$, $m = 0.1$; d) $\lambda = 10$, $m = 1$.

visco-elastic fluids. The key principles of this technique are as follows.

1. Lubricate the fluid layer with a layer of yield stress fluid, whilst ensuring that the base flow retains an unyielded plug at the interface, (type I flows). This has the effect of stabilizing interfacial instabilities.

2. Select the flow and rheological parameters so that the interfacial velocity (equivalently plug velocity) exceeds a critical cut-off velocity. This cut-off velocity is determined from study of the PCP flow of the lubricated fluid on alone, in a channel with moving lower wall. The cut-off velocity is that at which the Couette component becomes strong enough to stabi-

lize all long wavelength instabilities, which are typically the least stable.

As we have seen, there are relatively large parameter regimes in which these effects can be achieved. Although for simplicity we have only identified the regime where $Re = \infty$ is stable, note that as this boundary is approached, i.e. from within the black shaded area of Figs. 6 & 8, the stability typically increases from that of the plane Poiseuille flow as soon as the interfacial speed exceeds the wave speed of the least stable modes (this is found to be when long wavelengths become the least stable). In contrast, at the boundaries of the stable type I

region with the type III and type IV flows, the interface becomes yielded, so the stability is lost.

Before considering practical limitations of these results, let us first discuss their generality. We have chosen the Carreau fluid as a generic shear-thinning generalised Newtonian fluid. Other models, e.g. power law, might be easier to handle analytically, i.e. in terms of computing the base flows, but are sometimes limited in their range of applicability. In particular it is common to have shear-thinning behaviour dominant over a range of lower shear rates coupled with an asymptotic approach to some high shear plateau. We suspect that the stability behaviour is qualitatively similar for all such fluids, e.g. that the PCP flow will have a cut-off velocity, and therefore that our results are quite generic. On the other hand, the visco-elastic model we have chosen is less generic. This model includes the Oldroyd B and is closely related to other FENE type models. Therefore, we would not be surprised to find similar cut-off behaviour for the PCP flow of similar fluids and hence regions of stability at $Re = \infty$. This remains however to be investigated. The MCR fluid has Newtonian shear viscosity and could be varied to include more realistic shear-thinning effects. We do not expect that this will change the qualitative nature of our results. Lastly, we could of course extend these flows to different types of yield stress fluid and again do not expect significant qualitative differences.

There are different arenas for the application of the technique put forward here. Firstly, if either of the flu-

ids is interpreted as a coating and/or if a multi-layered structure is the end goal, then the method implies stable flows at high throughput. Alternatively, the yield stress fluid may be thought of as a lubricant. In this setting one augments the volumetric flux at the cost of the lubricating fluid layer. Although we can of course calculate the consumption of the lubricant as a function of the increase in flow rate this is not the main focus here. For the MCR fluid, where the base flow is Newtonian, the increase in flow rate is simply due to the moving interface, (i.e. found by superimposing a Couette component), so that increased flow stability coincides with an increased flow rate! For shear thinning fluids the additional shear results in relatively larger Couette components.

There are many practical limitations to be acknowledged. First, the domain is a geometric idealisation of a planar geometry of large aspect ratio. Depending on the actual geometry it becomes necessary to consider other effects, e.g. entry/start-up effects of the flow, curvature or imperfections of the walls, etc.

Secondly, even allowing for the geometric limitations, linear stability at $Re = \infty$ needs interpreting cautiously. Linearly stable flows frequently are unstable to finite perturbations at significantly lower Re than their linear limit, e.g. plane Poiseuille flow and Hagen-Poiseuille flow for Newtonian fluids. The same is probably true for inelastic shear-thinning models. Regarding the lubricating yield stress fluid layer, there are relatively few studies of nonlinear instability for these fluids, e.g. [1,4], and fewer

still with an interface and multiple fluids, e.g. [2]. In the visco-elastic context Pakdel and McKinley have advanced an argument that relates the critical Weissenberg number for instability to the characteristic curvature of the flow streamlines, [5]. Whilst apparently irrelevant to planar flows such as here, Saarloos and co-workers have recently advanced the notion that the critical curvature may be related to the amplitude of a finite perturbation. Thus, both plane Couette flow and (pipe) Poiseuille flow have been shown to exhibit weakly nonlinear subcritical instabilities; see [7,6,8]. The critical amplitude at which instabilities are found decreases with increasing Weissenberg number.

On the other hand in the experimental setting, for flows that are linearly stable at $Re = \infty$ the point at which instability is actually observed is very sensitive to control of apparatus imperfections and the level of flow perturbations. For example, in Hagen-Poiseuille flow of Newtonian fluids one typically observes transition to turbulence starting for $Re \gtrsim 2000$. However, an experimental flow loop in Manchester UK produces stable laminar flows for $Re \approx 24,000$, [32,33], and stable flows have even been reported up to $Re \approx 100,000$, [34]. This suggests that enhanced stability may be achieved experimentally, where predicted by the linear theory.

The other experimental aspect where our theoretical predictions may fail is if the unyielded plug region at the interface is disturbed by some means. Although we have not conducted experiments in the configuration considered, those in [3] utilised Xanthan and Carbopol solutions in a core-annular configuration and observed no disruption of the interface until the onset of shear instabilities in the core fluid. Current experimental work is focused at a PEO-Carbopol system in the same apparatus.

A more serious barrier to linear stability at $Re = \infty$ comes with remaining within the correct parameter regime. Increased Re often implies an increased velocity U_{max}, but the Bingham number then decreases, potentially moving out of the Type I base solution regime.

References

1. C. Nouar and I.A. Frigaard, J. Non-Newt. Fluid Mech., **100,** (2001) 127–149.

2. M. Moyers-Gonzalez, I.A. Frigaard and C. Nouar, J. Fluid Mech., **506,** (2004) 117–146.

3. C.K. Huen, I.A. Frigaard and D.M. Martinez, J. Non-Newt. Fluid Mech., **142,** (2007) 150-161.

4. C. Metivier, PhD Thesis, LEMTA, Nancy, (2007).

5. P. Pakdel and G.H. McKinley, Phys. Rev. Lett., **77,** (1996) 2459–2462.

6. B. Meulenbroek, C. Storm, V. Bertola, C. Wagner, D. Bonn and W. van Saarloos, Phys. Rev. Lett., **90,** (2003) 024502.

7. V. Bertola, B. Meulenbroek, C. Wagner, C. Storm, A.N. Morozov, W. van Saarloos and D. Bonn, Phys. Rev. Lett., **90,** (2003) 114502.

8. A.N. Morozov and W. van Saarloos, Phys. Rev. Lett., **95,** (2005) 024501.

9. S.A. Orszag, J. Fluid Mech., **50,** (1971) 689–703.

10. V.A. Romanov, Funct. Anal. Appl., **7,** (1973) 137–146.

11. C.-S. Yih, J. Fluid Mech., **27,** (1967) 337–352.

12. C. Hickox, Phys. Fluids, **14,** (1971) 251–262.

13. D. Joseph and Y. Renardy, *Fundamentals of Two-Fluid Dynamics*, (Interdisciplinary Applied Mathematics, Springer, 1993).

14. E. Hinch, J. Fluid Mech., **114,** (1967) 463–465.

15. F. Charru and E. Hinch, J. Fluid Mech., **414,** (1967) 195–223.

16. P. Ern, F. Charru and P. Luchini, J. Fluid Mech., **496,** (1967) 295–312.

17. N.D. Waters, J. Non-Newt. Fluid Mech., **12**, (1983) 85–94.

18. N.D. Waters and A.M. Keeley, J. Non-Newt. Fluid Mech., **24**, (1987) 161–181 .

19. B. Khomami, J. Non-Newt. Fluid Mech., **36**, (1990) 289–303.

20. Y. Y. Su and B. Khomami, Chem. Eng. Comm., **109**, (1991) 209–223.

21. A. Pinarbasi and A. Liakopoulos, J. Non-Newtonian Fluid Mech. **57**, (1995) 227–241.

22. J. Remmelgas, P. Singh and L.G. Leal, J. Non-Newtonian Fluid Mech., **88,** (1999) 31–61.

23. M. Sahin and R.G. Owens, J. Non-Newtonian Fluid Mech., **123,** (2004) 121–139.

24. I.A. Frigaard, S.D. Howison and I.J. Sobey, J. Fluid Mech., **263,** (1994) 133-150.

25. I.A. Frigaard, J. Non-Newtonian Fluid Mech., **100,** (2001) 49–76.

26. C. Nouar, N. Kabouya, J. Dusek and M. Mamou, J. Fluid Mech., **577,** (2007) 211-239.

27. M.A. Moyers-Gonzalez and I.A. Frigaard, J. Non-Newtonian Fluid Mech., accepted November 2009 and to appear.

28. M.C. Potter, J. Fluid Mech., **156,** (1985) 83–100.

29. F.D. Hains, Phys. Fluids, **10,** (1966) 2079–2080.

30. S.J. Cowley and F.T. Smith, J. Fluid Mech., **156,** (1985) 83–100.

31. C. Nouar and I.A. Frigaard, Phys. Fluids, **21,** (2009) 064104.

32. B. Hof, C.W.H. vanDoorne, J. Westerweel, F.T.M. Nieuwstadt, H. Faisst, B. Eckhardt, H. Wedin, R.R. Kerswell and F. Waleffe, Science, **305,** (2004) 1594–1598

33. J. Peixinho and T. Mullin, Phys. Rev. Lett., **96,** (2006) 094501.

34. W. Pfenniger, in *Boundary Layer and Flow Control*, G.V. Lachman, Ed. (Pergamon, Oxford, 1961), 970-980.